THE JOURNAL OF PHYSICAL CHEMISTRY LETTERS
A JOURNAL OF THE AMERICAN CHEMICAL SOCIETY

pubs.acs.org/JPCL

Perspective

Continuously Graded Quantum Dots: Synthesis, Applications in Quantum Dot Light-Emitting Diodes, and Perspectives

Yang Cheng, Haoyue Wan, Tianyu Liang, Can Liu, Muhong Wu, Hao Hong,* Kaihui Liu,* and Huaibin Shen*

Cite This: *J. Phys. Chem. Lett.* 2021, 12, 5967−5978

Read Online

ACCESS | Metrics & More | Article Recommendations

ABSTRACT: Colloidal quantum dot (QD) light-emitting diodes (QLEDs) hold the promise of next-generation displays and illumination owing to their excellent color saturation, high efficiency, and solution processability. For achieving high-performance light-emitting diodes (LEDs), engineering the fine compositions and structures of QDs is of paramount importance and attracts tremendous research interest. The recently developed continuously graded QDs (cg-QDs) with gradually altered nanocompositions and electronic band structures present the most advanced example in this area. In this Perspective, we summarize the current progress in LEDs based on cg-QDs, mainly concentrating on their synthesis and advantages in addressing the great challenges in QLEDs, like efficiency roll-off at high current densities, short operation lifetimes at high brightness, and low brightness near the voltage around the bandgap. In addition, we propose accessible approaches exploiting the cutting-edge mechanisms and techniques to further optimize and improve the performance of QLEDs.

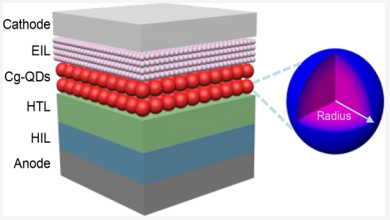

Quantum dots (QDs) with typical core/shell structures have aroused extensive attention because of their unique optical properties, such as tunable emission wavelength, high photoluminescence (PL) efficiency, spectral purity, and photostability.[1−5] Those considerable merits, together with the low-cost, reproducible ,and scalable fabrication techniques,[6,7] give QDs an enormous range of potential optical applications in solid-state lighting, displays, and lasers. QLEDs are the most representative ones which have been widely studied and put into commercial applications. Resulting from numerous devoted efforts since the first demonstration in 1994, the external quantum efficiencies (EQEs) of QLEDs have been elevated to a near-theoretical-maximum of ∼20%. The superior performance guarantees the success of QLEDs in mobile displays and television screens (<1000 cd m^{-2}).[8−17]

However, the performance of LEDs based on traditional core/shell QDs decreases dramatically at high brightness, which limits their widespread applications: the EQE deteriorates obviously with brightness/current density increases (the so-called efficiency roll-off);[18−20] the short T_{95} operation lifetimes (the time for the device to decrease to 95% of the initial brightness under 1000 cd m^{-2}) is far below the 10 000 h requirement for display applications at high initial brightness.[21−24] Furthermore, minimizing the near-bandgap voltage of QLEDs with high efficiency and high brightness simultaneously and realizing QD-based laser diodes with direct-current electrical pumping are still long-standing challenges in future applications based on core/shell QDs for displays and lasers.

The nonradiative Auger recombination, which stems from the mutiexcitonic nature, defect trapping, excess carriers, etc., is believed to be the main obstacle accounting for these challenges.[25−27] To suppress the Auger recombination for minimizing or even eliminating the efficiency roll-off, tremendous efforts have been made, such as increasing the shell thickness, passivating the trap states at the surface, and improving the charge injection balance.[28−35] Recently, cg-QDs with smooth confinement potential (Figure 1a) hold the promise of effectively minimizing the nonradiative Auger recombination, like suppressing the intraband transition of the extra carrier during the Auger processes and substantially balancing charge injection in QLEDs resulting from the fine nanostructures of the cg-QDs (Figure 1b).[36−38] Utilizing the successful experiences based on core/shell QDs, we anticipate the nearly droop-free, high-efficiency, and high-brightness cg-QD LEDs can facilitate the development of electroluminescent full-color display and solid-state lighting applications.[39−41]

In this Perspective, we address the great potential of cg-QDs for high-quality display, lighting, and lasing technologies. First, we show the current synthesis of cg-QDs can be mainly divided into two categories. Then, we introduce the enormous challenges met in the current QLED applications. Furthermore, we demonstrate the great potential of cg-QDs for resolving the above problems and illustrate the underlying

Received: May 16, 2021
Accepted: June 17, 2021
Published: June 23, 2021

https://doi.org/10.1021/acs.jpclett.1c01554
J. Phys. Chem. Lett. 2021, 12, 5967−5978

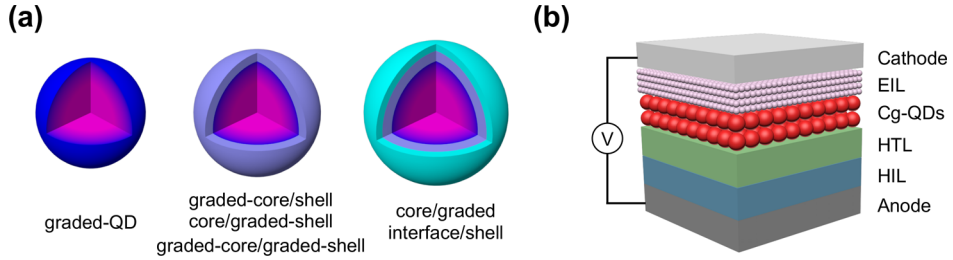

Figure 1. Schematics of cg-QDs and QLEDs. (a) Schematics of three types of cg-QDs: the QDs are continuously graded along the whole radial direction, one or both of the core and shell of QDs are continuously graded along the radial direction, and the continuously graded intermediate layer is between the core and the shell of QDs, respectively. (b) Schematics of typical QLEDs based on cg-QDs.

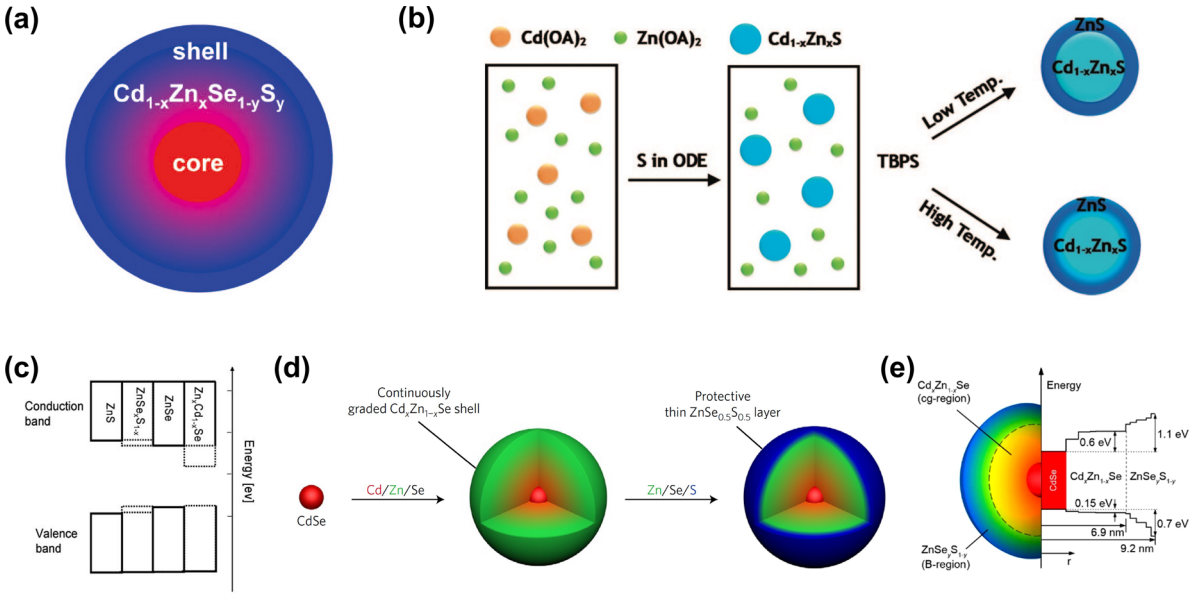

Figure 2. Fabrication methods of cg-QDs. (a) One-step synthesis of $Cd_{1-x}Zn_xSe_{1-y}S_y$ cg-QDs with continuously graded nanocompositions along the whole radial direction. Reprinted from ref 42. Copyright 2008 American Chemical Society. (b) Schematic illustration of continuously graded $Cd_{1-x}Zn_xS$ cores with ZnS shell. The smoothness of the core/shell interface can be adjusted by changing the reaction temperatures during shell growth. Reprinted from ref 47. Copyright 2008 American Chemical Society. (c) The energetic band alignments of $Zn_{1-x}Cd_xSe/ZnSe/ZnSe_xS_{1-x}/ZnS$ QDs. Reprinted from ref 44. Copyright 2011 The Royal Society of Chemistry. (d) Reaction schematics of $CdSe/Cd_xZn_{1-x}Se/ZnSe_{0.5}S_{0.5}$ QDs with multistep synthesis. Reprinted from ref 48. Copyright 2017 Springer Nature. (e) Structures and band alignments of $CdSe/Cd_xZn_{1-x}Se/ZnSe_yS_{1-y}$ QDs. Reprinted from ref 49. Copyright 2018 American Chemical Society.

mechanisms. Finally, we give our perspectives on the further optimizations of QLEDs based on cg-QDs.

The Synthesis of cg-QDs. The emergence of cg-QDs which utilize and optimize the chemical principles derived from the synthesis of heterostructural core/shell QDs has been widely applied to QLEDs and lasers. Here, we mainly focus on the synthesis of CdSe- and CdS-based core/shell cg-QDs which have the most mature fabrication processes and the most extensive applications.

To date, the CdSe- and CdS-based cg-QDs reported can be divided into three major categories: (1) QDs that are continuously graded along the whole radial direction, which means there is no obvious boundary between the core and shell layer (left panel in Figure 1a);[42,43] (2) one or both of the core and the shell of QDs are continuously graded along the radial direction (middle panel in Figure 1a);[44−49] (3) the continuously graded intermediate layer is between the core and the shell of QDs (right panel in Figure 1a).[50−53] It should be emphasized that, although the unintentional alloying of the core/shell interface had been realized in the early stages of QD synthesis,[54] now it is possible to precisely quantitatively control the element composition ratio and the thickness of cg-QD layers. To date, the composition of the cg-QD structures is tough to identify. As the activities of the precursor are different, the actual structures of QDs will deviate from the original design. More high-resolution characterization approaches, such as increasing the resolution of line scan of the energy dispersive X-ray spectroscopy, are in urgent need of research to provide QD fine structures.

In contemporary material science research, an effective, straightforward, and environmentally-friendly fabrication technique is the basic and fundamental procedure. There are two main methods successfully used in cg-QDs synthesis: one-step method and multistep method. The one-step method refers to adding all the reactants into the reaction flask at the same time to generate cg-QDs. In a typical one-step synthesis of cg-QDs, Se powder and S powder are injected into the clear solution of $Cd(OA)_2$ and $Zn(OA)_2$ simultaneously. Under their reaction conditions, the CdSe-based QDs have continuously graded structures ($Cd_{1-x}Zn_xSe_{1-y}S_y$) due to the varying reactivity of a mixture of precursors (Figure 2a).[42] The multistep method synthesizes cg-QDs with a core/shell structure step by step, for

https://doi.org/10.1021/acs.jpclett.1c01554
J. Phys. Chem. Lett. 2021, 12, 5967−5978

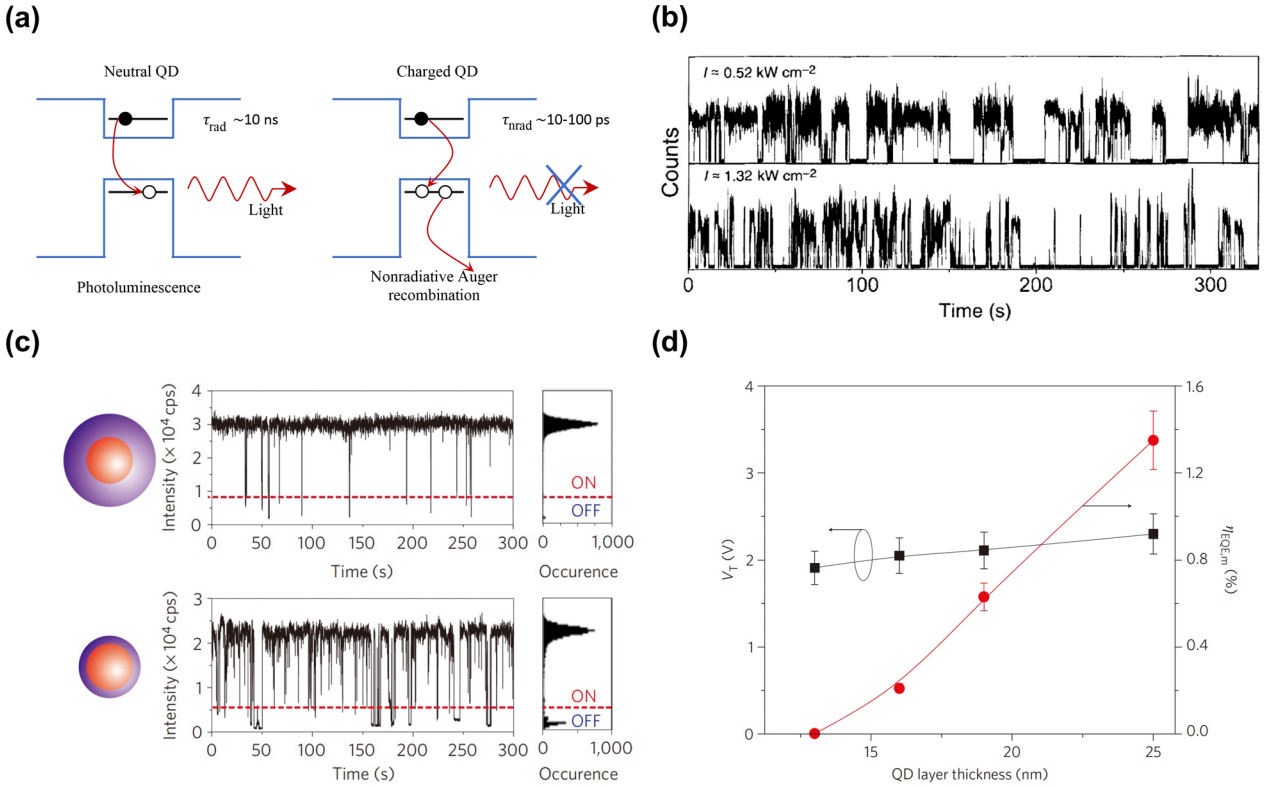

Figure 3. Auger processes in QDs and typical approaches to suppress it. (a) Schematic illustration of Auger processes. Left panel: the normal radiative recombination processes of electron−hole pair in a neutral QD with decay time τ_r on the order of 10 ns. Right panel: the Auger recombination processes of an electron−hole pair in a charged QD with decay time τ_{nr} on the order of 10−100 ps. (b) Comparison of fluorescence-intensity versus time traces at excitation intensities of ~0.52 and ~1.32 kW cm^{-2} with a sampling interval of 10 ms. Reprinted from ref 57. Copyright 1996 Springer Nature. (c) Top panel: PL blinking trace of a single CdSe/CdS core/shell QD with a CdSe core radius of 2.2 nm and a shell thickness of 2.4 nm (~7 monolayers). Bottom panel: same but with a shell thickness of 0.7 nm (~2 monolayers). Reprinted from ref 58. Copyright 2013 Springer Nature. (d) Turn-on voltage (V_T) and maximum EQE ($\eta_{EQE,m}$) versus QD layer thickness. Error bars represent variation about the average for 16 pixels on four devices, and each is typically less than ±10%. Reprinted from ref 13. Copyright 2011 Springer Nature.

example, preparing continuously graded $Cd_{1-x}Zn_xS$ cores first by introducing S precursors into the mixed solution of $Cd(OA)_2$ and $Zn(OA)_2$ and then successively overcoating ZnS shells on the $Cd_{1-x}Zn_xS$ cores by the second injection of S precursors (Figure 2b).[47] By adjusting the temperature of the shell growth, Bae et al. reported that the degree of continuity of the interface between the core and shell could be fully controlled. At lower temperatures, the $Cd_{1-x}Zn_xS$/ZnS interface has a sharp boundary (upper panel in Figure 2b), while at higher temperatures, Zn atoms in the ZnS shell can migrate into the core to form a continuous boundary (lower panel in Figure 2b). In addition to the growth of a noncontinuous shell onto the continuously graded core, Shen et al. reported that the continuously graded shell could be also successfully adding onto it (Figure 2c).[44] They employed the "successive ion layer adsorption and reaction" (SILAR) method to grow $ZnSe_yS_{1-y}$ shells on the $Zn_{1-x}Cd_xSe$ cores which showed enhanced PL stability and improved crystallinity.

Different from the method of growing a shell layer based on the continuously graded core, another widely used technique grows the shell layer directly on the noncontinuous core, which also presents excellent optical properties. Lim et al. synthesized continuously graded CdSe/$Cd_xZn_{1-x}Se$/$ZnSe_{0.5}S_{0.5}$ QDs that were expected to have great potential in lasers with direct-current electrical pumping (Figure 2d).[48] After dispersing the CdSe cores in a mixed solution and controlling the unceasing injection of reactants, they obtained a continuously graded $Cd_xZn_{1-x}Se$ shell on the CdSe core. In addition, they coated these CdSe/$Cd_xZn_{1-x}Se$ particles with a thin $ZnSe_{0.5}S_{0.5}$ outer shell to protect te QDs from degradation. The new type of multishell QDs comprising a CdSe core coated with a continuously graded $Cd_xZn_{1-x}Se$ inner shell followed by a barrier outer shell of $ZnSe_yS_{1-y}$ (Figure 2e) had been also proposed by Lim et al.[49] The $Cd_xZn_{1-x}Se$ inner shell was able to suppress the Auger recombination processes, and the $ZnSe_yS_{1-y}$ outer shell with a wide gap could optimize the injection of electrons and holes in QLEDs.

A novel synthesis for fabricating cg-QDs along the whole radial direction with a large size and nearly free of strain-induced defects still faces tremendous challenges and awaits opportunities in the future.[55]

Suppression of Auger Recombination Processes in cg-QDs. The nonradiative Auger recombination processes are quite universal and strongly enhanced in QDs compared to their bulk counterparts because of confined carrier wave function. In a neutral fluorescing QD, the electron−hole pair recombines and emits a photon (left panel in Figure 3a). However, when the QD is in a charged state or a multicarrier state, the energy released from the recombination of the electron−hole pair will be transferred to the extra carrier, either an electron or a hole (right panel in Figure 3a).[56] These nonradiative Auger recombination processes are much faster (τ_{nr} is about 10−100 ps) than the radiative recombination processes (τ_r is on the order of 10 ns),[37,56] which results in complete suppression

https://doi.org/10.1021/acs.jpclett.1c01554
J. Phys. Chem. Lett. 2021, 12, 5967−5978

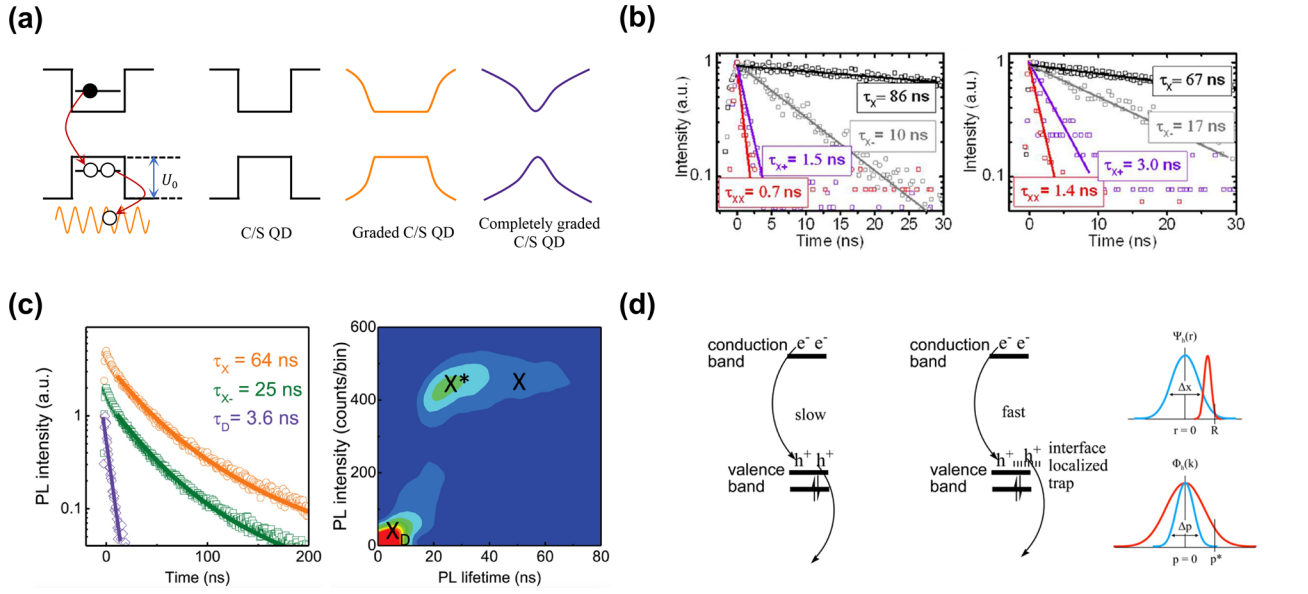

Figure 4. Effective suppression of Auger effect in cg-QDs. (a) Left panel: a schematic diagram showing Auger recombination processes where the remnant hole is ejected into the continuum. Middle to right panel: the schematics show different types of potential shapes from "abrupt" to "smooth". (b) PL intensity dynamics measured for individual CdSe/CdS and CdSe/CdSeS/CdS QDs. The neutral exciton, negative trion, positive trion, and biexciton dynamics included in these plots are shown with black, gray, purple, and red curves, respectively. Reprinted from ref 52. Copyright 2014 American Chemical Society. (c) The fluorescence-lifetime-intensity distribution plot reveals that the bright state is due to superposition of two high-emissivity, bright states (orange circles and green squares) of similar emissivities but different lifetimes. Reprinted from ref 53. Copyright 2017 American Chemical Society. (d) Left and center panels: mechanism for slow, band-edge and fast, trapped hole Auger relaxation, respectively. Right panel: schematic of band edge (blue) and trapped (red) wave functions in real (top panel) and momentum (bottom panel) space. The schematic shows the trapped hole has a much larger amplitude at p^* (the momentum of the hot hole). Reprinted from ref 61. Copyright 2016 American Chemical Society.

of the PL in charged QDs. A well-known result of the Auger effect is PL blinking, which was first observed in the single fluorescing nanocrystals of CdSe under continuous excitation (Figure 3b). Under higher excitation intensity, carriers are captured by the trapping sites because of the multiexciton effect, leaving the QDs ionized.[57] Thus, the Auger nonradiative recombination processes are strongly enhanced in charged QDs, causing the turning-off of luminescence.

An early attempt to suppress the Auger effect was to separate the photogenerated carriers from the trapping sites located at the QD surface by introducing a thick shell of a wide-gap material.[28−31] The PL blinking trace of a single CdSe/CdS QD with a thicker shell shows less PL quenching compared with the one with a thinner shell (Figure 3c).[58] In addition, the Auger effect in QLEDs can be suppressed by increasing the QD layer thickness (Figure 3d); the ultrafast charge transfer between the QD layer and the adjacent electron transport layer (ETL) can suppress the Auger recombination processes.[13,32]

Controlling the shape of the confinement potential is a more effective way to suppress the Auger effect. It was first proposed by Cragg and Efros that the Auger processes were strongly quenched in the structures with a soft confining potential.

The Auger rate $1/\tau_A$ can be calculated according to Fermi's golden rule

$$\frac{1}{\tau_A} = \frac{2\pi}{\hbar}|M_{if}|^2 \rho(E_f) \tag{1}$$

The electronic transition matrix element of the interparticle Coulomb interaction M_{if} can be derived as[36]

$$M_{if} \simeq \frac{e^2}{\kappa}\frac{\sqrt{2}}{2\pi}\psi_h^0(k_f)^* \int_{-1/a}^{1/a} dq\tilde{V}'(q) \tag{2}$$

$$\tilde{V}'(q) \propto \int_{-\infty}^{\infty} dx \exp(-iqx)\psi_h^0(x)^*\psi_e^0(x)^* \tag{3}$$

From eq 1, the Auger decay rate depends on both the overlap of the electron and hole envelope wave functions in $\tilde{V}'(q)$ and the overlap of the initial and final states of the third carrier in $\psi_h^0(k_f)$ (left panel in Figure 4a). While the former overlap can be reduced in type-II or quasi-type-II QDs,[59,60] the latter overlap can be controlled by designing the shape of the confinement potential. Because the third carrier is excited to a high-energy state, it acquires a large momentum.

Considering the overlap of the initial and final states of the carrier in momentum space, it depends on the high-frequency components in the ground states. For abrupt potential, it has large high-frequency components and thus a large overlap. However, if the potential is much smoother, the overlap can be significantly reduced. As a result, the Auger effect can be suppressed when we change the confinement structure from "abrupt" potential in core/shell QD to "smooth" potential in completely cg-QD (Figure 4a). This has been confirmed in several experimental studies by comparing core/shell QD with and without interfacial alloying.[50,51] Park et al. reported that all the lifetimes of positive trion, negative trion, and biexciton are about twice greater in continuously graded CdSe/CdSeS/CdS (C/A/S) QDs in comparison with those of CdSe/CdS (C/S) QDs by measuring their PL intensity dynamics, indicating the suppression of Auger effect (C/S and C/A/S QDs are represented in the left and right panels in Figure 4b, respectively).[52] Furthermore, the phenomenon of "lifetime blinking" which is usually caused by fluctuations between neutral exciton states (longer lifetime, X) and "Auger-decay free" trion states (shorter lifetime X*) also illustrates the

https://doi.org/10.1021/acs.jpclett.1c01554
J. Phys. Chem. Lett. 2021, 12, 5967−5978

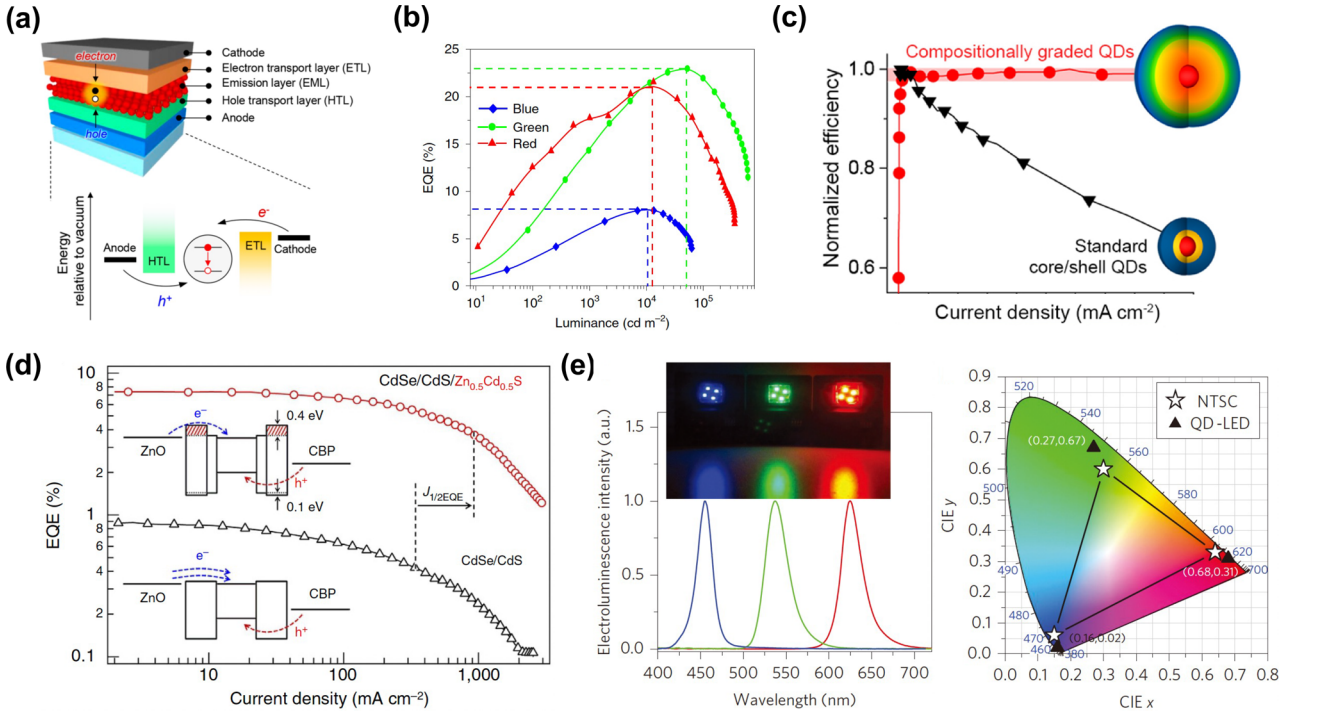

Figure 5. High-efficiency QLEDs based on cg-QDs. (a) Schematics of typical QLED structures and corresponding energetic band alignments of the different layers in QLEDs. Reprinted from ref 67. Copyright 2016 American Chemical Society. (b) Luminance-dependent EQEs for red, green, and blue QLEDs. The peak EQEs are highlighted using the dashed lines. Reprinted from ref 15. Copyright 2019 Springer Nature. (c) Schematics showing the efficiency roll-off at high current densities for standard core/shell QDs and cg-QDs with droop-free behaviors. Reprinted from ref 49. Copyright 2018 American Chemical Society. (d) Current-density-dependent EQEs of QLEDs with CdSe/CdS and CdSe/CdS/$Zn_{0.5}Cd_{0.5}S$ QDs, represented with black triangles and red circles, respectively. The EQE roll-off onsets at $J_{1/2EQE}$ are indicated with vertical dashed lines. Reprinted from ref 25. Copyright 2013 Springer Nature. (e) Left panel: the normalized EL spectra and optical images of blue, green, and red QLEDs. Right panel: the CIE coordinates of the blue, green, and red QLEDs (marked in triangles) compared with the National Television System Committee (NTSC) color standards (marked by stars). Reprinted from ref 32. Copyright 2015 Springer Nature.

strong suppression of nonradiative Auger decay of trion states (Figure 4c).[53] The lifetimes of the trion states are about half of the neutral exciton lifetimes, while their PL intensities are at the same level.

There are also some other theories explaining why the soft interface between the core and shell can suppress the Auger effect. Beane et al. suggested two types of biexciton processes to explain the effect of interface sharpness in controlling the excited-state dynamics in CdSe/ZnSe QDs (Figure 4d).[61] In the usual biexciton Auger processes (left panel in Figure 4d), the two holes are both in the band edge, which limit the Auger rate because of the momentum constraints. However, under the presence of the strain-induced defects at the core/shell interface, the holes will be captured and they are also involved in the Auger effect (center panel in Figure 4d). Because the trapped holes are extremely confined spatially, they largely relax the momentum constraints and boost the Auger effect (right panel in Figure 4d). However, for cg-QDs, the soft alloyed interface reduces much lattice strain and hence the probability of trapped holes causing suppression of the Auger effect in the cg-QDs.

Overall, the soft confinement potential in cg-QDs can significantly suppress the Auger effect and result in high PL efficiency with minimized PL blinking phenomenon in most cases.[51−53,62−65] Consequently, cg-QDs with the near-unity PL quantum yield, high brightness, and pure color have wide applications in QLEDs and lasers, paving the way toward next-generation displays and illumination.

High-Efficiency LEDs Based on cg-QDs. LEDs based on cg-QDs exhibit superior performance in thin-film displays and white-color illumination with high efficiency and brightness and long lifetimes. In a typical QLED device with the *p*-i-*n* structure, the QD emissive layers are usually sandwiched between aluminum and indium tin oxide (ITO) as the reflective and transparent electodes, respectively (Figure 5a).[66,67] In addition, the QLEDs have various functional layers in sequence: an electron injection layer (EIL), an ETL, an emitting layer (EML), a hole transport layer (HTL), and a hole injection layer (HIL). The corresponding schematic of the energy band diagram of different layers in a QLED is also shown in Figure 5a. According to the wavelength of light emission, the current QLEDs can be divided into red, green, and blue LEDs (Figure 5b).[15] When the QDs of red, green, and blue colors are mixed together, the white-color QLEDs can also be realized.[68−70] However, the current development status of red, green, and blue QLEDs is quite unbalanced. Particularly, the major challenge remaining in blue QLEDs is achieving high brightness and long operational lifetimes simultaneously, which can be overcome by engineering the structures of QDs, such as using cg-QDs in blue QLEDs. Recently, Shen et al. introduced a continuously graded layer between the core/shell interface and facilitated Se throughout the whole QDs. The lifetime of these blue QLEDs reached as high as 7000 h at 100 cd m^{-2}, which may result from charge carrier injection balance and high current densities at low voltages.[15]

https://doi.org/10.1021/acs.jpclett.1c01554
J. Phys. Chem. Lett. 2021, 12, 5967−5978

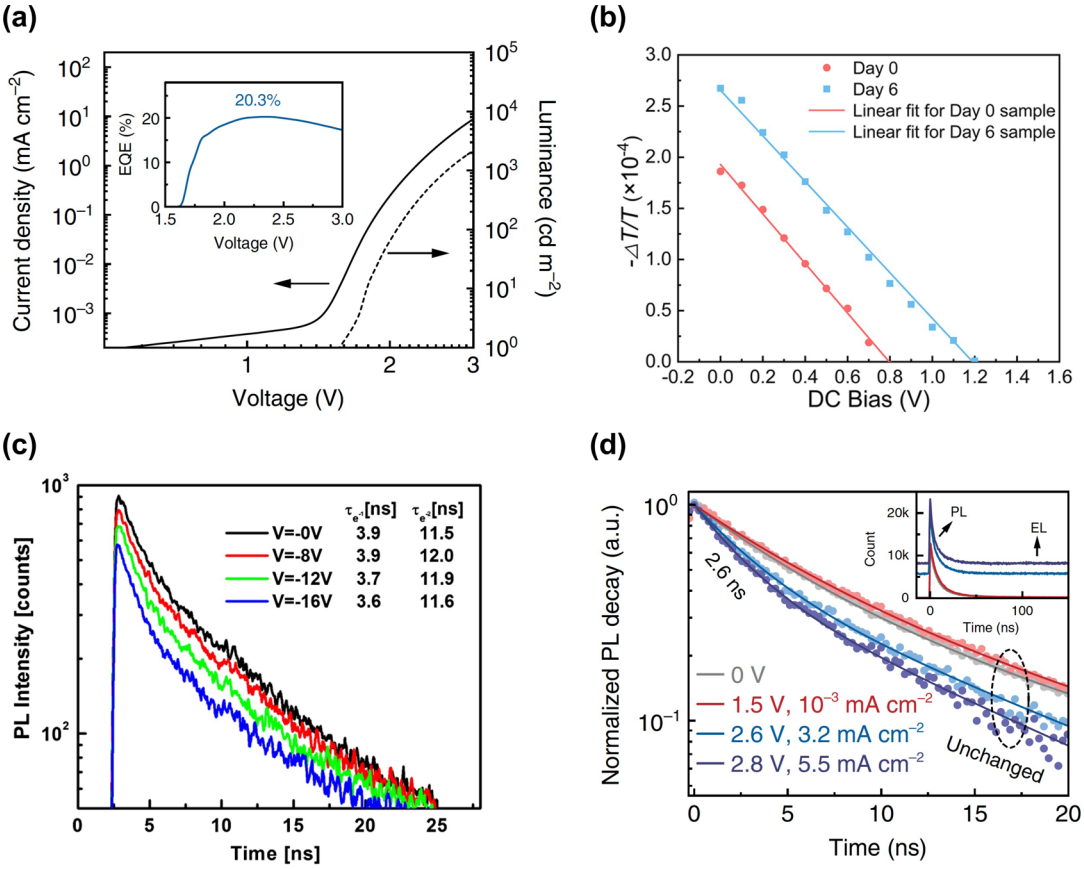

Figure 6. Characterization methodologies of QLEDs. (a) Luminance and current density versus voltage curves of QLEDs. Inset: the EQE versus voltage results. Reprinted from ref 73. Copyright 2020 Springer Nature. (b) Determination of the built-in potential using bias-dependent electroabsorption spectra of QLEDs after 7 days. Reprinted from ref 74. Copyright 2020 American Chemical Society. (c) Transient PL spectra of QLEDs at reverse bias. The fitting time constants of the decay curves are voltage-independent. Reprinted from ref 67. Copyright 2013 American Physical Society. (d) Transient PL spectra of QLEDs driven at different voltages. Inset: the original time-correlated single-photon-counting data of PL and EL. Reprinted from ref ref 73. Copyright 2020 Springer Nature.

The EQE, defined as the ratio of the number of photons emitted from the device to the number of injected e−h pairs, is the key metric representing the performance of a QLED, which is mainly related to the QD PL quantum yield (η_{PL}) and the specific structure of a QLED. Outstanding challenges such as efficiency roll-off at high current densities, low brightness at around the bandgap, and the short lifetimes at high brightness severely limit the further achievable applications in displays. The emergence of cg-QDs with near-unity PL quantum yield, high brightness, and weakened Auger recombination processes is expected to be successfully applied in LEDs and resolve the problems mentioned above (Figure 5c).[49]

The physical understanding of the efficiency roll-off mechanisms in QLEDs has remained unclear. Reduction in electroluminescence (EL) efficiency due to the exciton dissociation under high electric field (quantum-confined Stark effect, QCSE), charge carriers leaking out of the QD layers, and Joule heating are possible causes for the efficiency roll-off in QLEDs. However, the nonradiative Auger recombination processes which can be due to either the intrinsic properties in QDs (like trapping sites at the surface or core/shell interface) or imbalance in electron and hole injection rates in devices have been proposed to be the main reason for the efficiency roll-off in QLEDs. Because the combination of materials involved in the device architecture has been proven to be effective and stable in QLEDs, a more practical technique to optimize the balance of charge injection is to subtly change the QD structure instead of redesigning the device structures of QLEDs.

Bae et al. reported that, by adding a continuously graded $Zn_{0.5}Cd_{0.5}S$ outer shell on the CdSe/CdS QD, the electron injection into the QD would be partially impeded on account of the increase of the conduction band edge. As a result, the peak EQE and the voltage of efficiency roll-off in LEDs based on cg-QDs are both larger than those of conventional QDs (Figure 5d).[25] Lim et al. also confirmed that utilizing continuously graded $Zn_{1-x}Cd_xS$ layer could suppress the QD charging and Auger recombination processes.[46] To further achieve LEDs based on cg-QDs with excellent performance, Song et al. reported that, by utilizing the continuously graded $Zn_{1-x}Cd_xSe/ZnSe/ZnS$ QDs, the QLEDs exhibited high peak EQE, high brightness, and very low efficiency roll-off at high current densities.[41]

High efficiency, high brightness, saturated pure colors, and long-lived lifetimes are all important parameters to determine the performance of QLEDs. LEDs based on cg-QDs not only possess minimized roll-off resulting from suppressed Auger effect but also have similar or even superior performances in comparison with current QLEDs. In addition to minimizing the issue of efficiency roll-off, LEDs based on cg-QDs can also improve the stability and prolong the lifetimes by reducing the Auger heating because of the suppression of Auger

https://doi.org/10.1021/acs.jpclett.1c01554
J. Phys. Chem. Lett. 2021, 12, 5967−5978

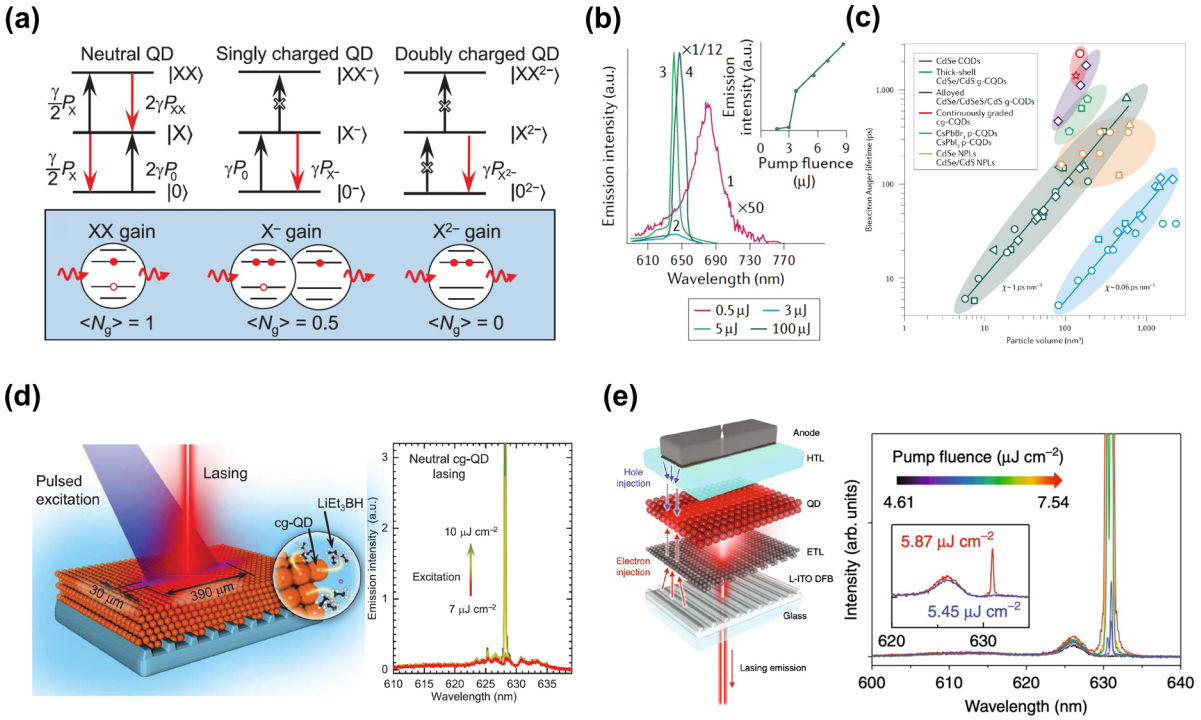

Figure 7. Lasers based on cg-QDs. (a) Top panel: schematics of the model of 2-fold degenerate states showing the principles of QD lasing. Bottom panel: the optical-gain threshold would be reduced by doping the QD with extra electrons. Reprinted from ref 79. Copyright 2019 Science. (b) First observation of optical gain and ASE in CdSe nanocrystals by ultrafast transient absorption studies. Reprinted from ref 78. Copyright 2021 Springer Nature. (c) The particle-volume-dependent biexciton Auger lifetimes $\tau_{A,XX}$ for various kinds of colloidal nanocrystals. Reprinted from ref 78. Copyright 2021 Springer Nature. (d) Left panel: the schematics of a distributed feedback (DFB) laser based on cg-QDs. Right panel: the emission spectra of the neutral cg-QD/DFB device showed a sharp transition to single-mode lasing when increasing the excitation fluences. Reprinted from ref 79. Copyright 2019 Science. (e) Left panel: the schematics of proposed QD laser diode architecture. Right panel: the pump fluence-dependent emission spectra of the L-ITO-based device showed the single-mode lasing when the pump fluence reaches the lasing threshold. Reprinted from ref 81. Copyright 2020 Springer Nature.

recombination processes.[71,72] Yang et al. revealed that the cg-QD-based LEDs could have narrow EL full width at half-maximum (fwhm) and saturated pure colors for all colors, as can be seen from the EL spectra and the Commission Internationale de l'Eclairage (CIE) chromaticity diagram shown in Figure 5e.[32]

Characterization Methodologies of QLEDs. Apart from the ingenious design of QLEDs, there has been a number of excellent contributions regarding the physics and advanced characterization methodologies of QLEDs in the past few years. The regular characteristics of QLEDs include the luminance−current density−voltage characteristics and EL spectra at varied voltages. The EQE−voltage and EQE−current density curves can be extracted from these results (Figure 6a).[73] The bias-dependent electro-absorption measurements can be carried out to measure the built-in potential of QLEDs to monitor the current injection efficiency. Zhang et al. measured the bias-dependent electro-absorption spectra of QLEDs after aging for 6 days.[74] They found that the built-in potential (V_{bi}) of QLEDs increased by ∼0.4 V, indicating the decrease in the work function of electrodes (Figure 6b).

The simultaneous EL−PL experiment can be performed to monitor the bias-dependent PL efficiency of QLEDs. Shirasaki et al. investigated the origin of efficiency roll-off in LEDs based on CdSe/ZnCdS core/shell QDs using EL−PL measurements.[18] Through the comparison of bias-dependent EL and PL of QLEDs, they found that the roll-off behavior of their QLEDs mainly resulted from the electric-field-induced QCSE (Figure 6c). Recently, Deng et al. developed electrically pumped single-nanocrystal spectroscopy to decipher exciton-generation processes in QD EL (Figure 6d).[73] They illustrated that the intermediate state of EL in the QLED was a negatively charged state (QD^-) according to the time-correlated single-photon-counting results. Combined with the PL−EQE−current density characteristics of QLEDs, they proposed that the long-lived intermediate QD^- state facilitated the hole injection efficiency.

These systematic and efficient approaches are of great significance for the characterization of the physical properties and performances of cg-QD LEDs.

Lasers Based on cg-QDs. Owing to the flexible size- and/or composition-tunable emission wavelength and high-temperature stability, QDs have also been widely used as the optical-gain media in laser applications.[75,76] The development of QD lasers has grown rapidly since the optical gain and the amplification by stimulated emission (ASE) in QDs were first observed by ultrafast transient absorption studies of CdSe nanocrystals (Figure 7b).[77,78] The principles of QD lasing can be illustrated with the model of 2-fold degenerate states (ground state $|0\rangle$, single-exciton $|X\rangle$, and biexciton $|XX\rangle$ states), wherein the probability difference of stimulated biexciton state in the conduction band (P_{xx}) and ground state in the valence band (P_0) is directly related with the optical gain threshold (top panel in Figure 7a).[79] Wu et al. uncovered that the optical-gain threshold, which was generally measured quantitatively with the average number of per-dot

https://doi.org/10.1021/acs.jpclett.1c01554
J. Phys. Chem. Lett. 2021, 12, 5967−5978

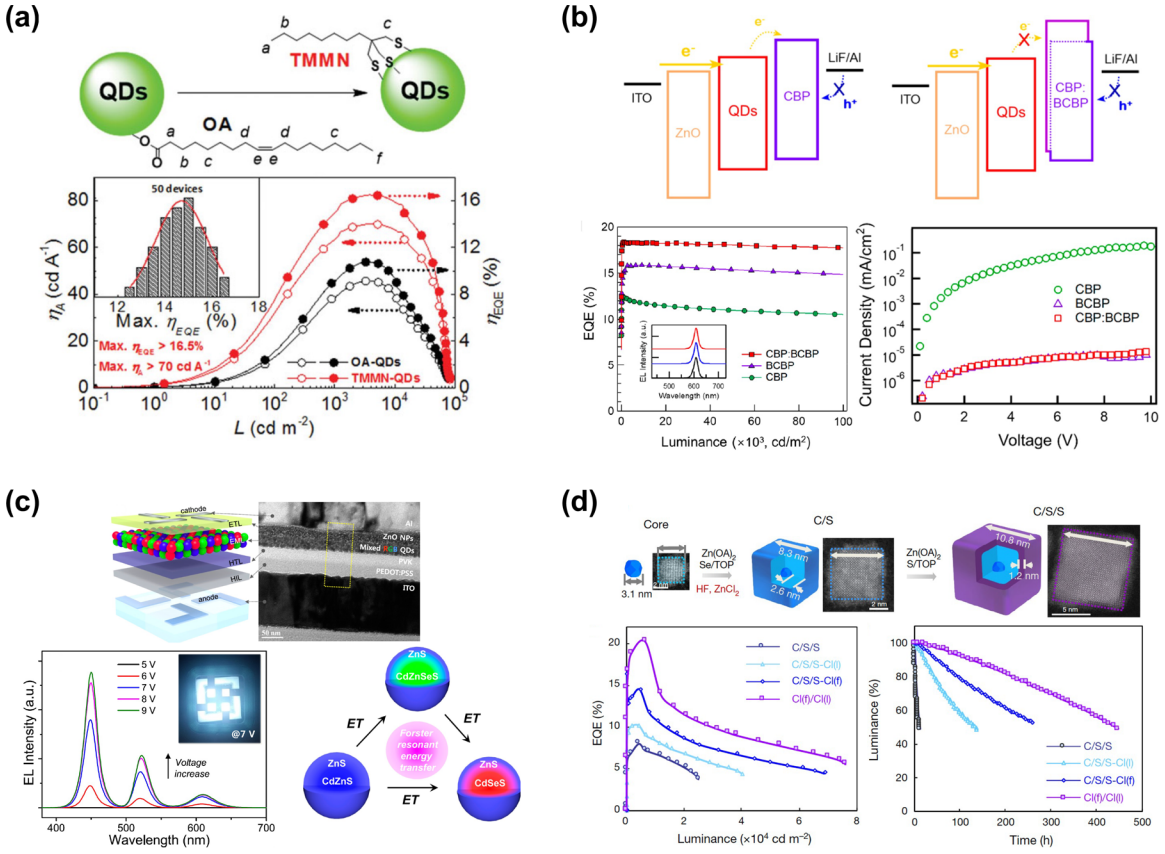

Figure 8. Feasible approaches to optimize QLEDs based on cg-QDs. (a) Top panel: QD with a new TMMN ligand. Bottom panel: EQE and current efficiency of OA QLEDs and TMMN QLEDs as a function of luminance. Inset: maximum-EQE distribution of 50 TMMN QLEDs. Reprinted from ref 33. Copyright 2016 John Wiley and Sons. (b) Top panel: electron flow schematics of CBP and BCBP:CBP HTL in electron-only devices (EODs), respectively. Bottom panel: luminance-dependent EQEs in QLEDs and voltage-dependent current density in EODs of CBP:BCBP, BCBP, and CBP HTLs. Reprinted from ref 34. Copyright 2020 American Chemical Society. (c) Top panel: the structure diagram and transmission electron microscopy micrograph of trichromatic QLEDs, respectively. Bottom left panel: spectrum of white-color QLEDs with a formulation reducing red QDs. Bottom right panel: schematic of FRET effect between three types of QDs in the EML. Reprinted from ref 70. Copyright 2015 American Chemical Society. (d) Top panel: schematic diagram of the synthesis of continuously graded ZnTeSe/ZnSe/ZnS QDs. Bottom left panel: EQE−luminance characteristics of different QLEDs optimized by ligand exchange based on cg-QDs. Bottom right panel: T_{50} operation lifetimes of QLEDs at 650 cd m^{-2} initially. Reprinted from ref 99. Copyright 2020 Springer Nature.

excitons ($\langle N_g \rangle$), would be reduced by doping the QDs with extra electrons (bottom panel in Figure 7a).[38] Nonetheless, the charging of QDs may lead to nonradiative multicarrier Auger decay simultaneously, which is still an enormous challenge for QD lasers.[80]

Cg-QD lasers offer immense potential in suppressing the Auger recombination processes of charged QDs through smoothing the confinement potential. The biexciton Auger lifetimes of cg-QDs are much slower than other types of colloidal nanocrystals, thereby impeding the Auger recombination processes (Figure 7c).[78] Kozlov et al. revealed that the photochemical charging and utilization of cg-QDs (CdSe/$Cd_xZn_{1-x}Se$/$ZnSe_{0.5}S_{0.5}$/ZnS) in lasers could hinder the Auger recombination processes and decrease the lasing threshold because of suppression of ground-state absorption (Figure 7d).[79] Lim et al. also observed optical gain in continuously graded CdSe/$Cd_xZn_{1-x}Se$/$ZnSe_{0.5}S_{0.5}$ QDs realized with the direct-current electrical pumping due to considerable suppression of the Auger recombination processes.[48] Recently, the optical-gain layer based on continuously graded CdSe/$Cd_xZn_{1-x}Se$/$ZnSe_{0.5}S_{0.5}$/ZnS QDs has been employed to fabricate devices that can operate as both an optically pumped laser and an LED, as proposed by Roh et al. (Figure 7e).[81] The superiorities of cg-QD lasers with the strongly reduced Auger recombination processes and the lengthening of the gain lifetimes will facilitate the lasers with entirely electrical-current pumping and provide giant opportunities for novel lasing mechanisms.

Conclusion and Perspectives. Given the excellent optical properties of cg-QDs and their successful implementation in LED applications, QLEDs can be used in many situations instead of organic LEDs (OLEDs). However, there are still many cutting-edge developments and ideas which can be used to enhance the performances of QLEDs. We give out four feasible aspects to optimize the QLEDs based on cg-QDs for next-generation displays and illumination.

Passivating the Surface Trap States of cg-QDs. Stacking faults and surface defects are major issues preventing the EQE and PL quantum yield of QLEDs from reaching their limits. Therefore, the performance of QLEDs can be enhanced via passivating the surface trap states. It has been reported that when CdSe QDs are exposed to moisture and light, the absorbed water molecules can passivate surface trap states and enhance PL quantum yield.[82,83] In addition, photoexcited QDs undergoing surface oxidation after being exposed to oxygen can also passivate the surface trap states.[84] Another approach

https://doi.org/10.1021/acs.jpclett.1c01554
J. Phys. Chem. Lett. 2021, 12, 5967−5978

through ligand design can also reduce fragile dangling bonds and stabilize the QD surface to enhance the properties of QLEDs.[85,86] Li et al. produced green QDs with tris-(mercaptomethyl)nonane (TMMN) ligand by ligand exchange (top panel in Figure 8a).[33] QLEDs with the new ligand showed higher EQE and current efficiency in comparison with long-chain oleic acid (OA)-coated QLEDs (bottom panel in Figure 8a). In addition, the EQEs of TMMN QLEDs also showed excellent reproducibility (bottom inner panel in Figure 8a).

Passivating the trap states at the surface of QDs can effectively increase the EQE and brightness of QLEDs, because electrons can be excited from the trap states to the conduction band of the QDs and the band-edge radiative recombination processes will be increased. Taking advantage of the techniques of photochemically passivating the trap states in cg-QDs, the QLEDs with high brightness and long lifetimes will achieve extraordinary development in the near future.

Tailoring the Electronic Band Structures of cg-QDs and QLEDs. The charge injection imbalance influences the efficiency of QLEDs in many aspects: the efficiency roll-off in QLEDs, increased Auger recombination processes, and irreversible structural damage of organic HTLs.[87,88] By tailoring the electronic band structures of both cg-QDs and QLEDs, the imbalance of charge injection can be reduced so as to enhance the performances of QLEDs. Rhee et al. designed the bright and stable QLEDs with harmonized charge injection rates based on CdSe/Cd_xZn_{1-x}Se-ZnSe/ZnS cg-QDs.[34] They purposefully engineered HTLs with codeposited mixtures (2,2′-bis(4-(carbazol-9-yl)phenyl)biphenyl (BCBP) and 4,4′-bis(*N*-carbazolyl)-1,1′-biphenyl (CBP)) to take advantage of both materials and enhanced the maximum EQE, current density, and stability of the device (bottom panel in Figure 8b). The increase of hole injection rates together with impeding the electron injection rates due to the energy upshift of the lowest unoccupied molecular orbital (LUMO) actually enhanced the charge injection balance (top panel in Figure 8b). Bae et al. also reported that the CdSe/CdS/$Zn_{0.5}Cd_{0.5}$S QDs could improve the charge injection balance by partially impeding the electron injection rates.[25] It is expected that more approaches can be used to resolve the imbalance of charge injection rates and to enhance the efficiency of QLEDs by subtly changing the nanocompositions of cg-QDs and the structures of current QLEDs.

Engineering White-Color LEDs with cg-QDs. White-color QLEDs with simple device architectures and inexpensive solution-processable fabrication techniques are expected to be powerful candidates to manufacture large-area plane light sources.[68,69] Lee et al. fabricated white-color QLEDs containing RGB QD-mixed multilayer EMLs by spin-casting a blend QD solution (red, green, and blue QDs were mixed together), which emitted perfect white light with a color gamut reaching 126% compared with the NTSC triangle standard (bottom left panel in Figure 8c).[70] The device structure and corresponding cross-sectional transmission electron microscopy micrograph of white-color QLEDs are presented in the top panel in Figure 8c. The white-color QLEDs with RGB QD-mixed layers utilize the Forster resonance energy transfer (FRET) effect that the blue QDs with highest-bandgap serve as the donor and the red QDs with the lowest bandgap serve as the acceptor, with the green QDs with intermediate bandgap filling both roles (bottom right panel in Figure 8c). Compared with the state-of-the-art white-color LEDs based on perovskites with a continuous and smooth spectrum together with the high brightness close to the natural sunlight,[89] white-color QLEDs have only a discrete multimodal spectrum. White-color QLEDs based on cg-QDs are expected to promote novel mechanisms and improve the device performances; for example, large cg-QDs in white-color QLEDs can well separate QDs from each other to decrease the FRET effect and optimize the hole injection rates by easily adjusting their nanocompositions to increase the maximum EQE.[90,91]

Environmentally-Friendly Cd-Free cg-QDs. Cd-based QDs are widely used and exhibit excellent properties. However, Derfus et al. showed that CdSe QDs would cause cytotoxicity by the free Cd^{2+} coming from the deterioration of CdSe when they were used for biological labeling.[92] In the context of the global environmental crisis, scientists are trying to produce Cd-free QDs. Many kinds of heavy-metal-free QLEDs have been designed, such as InP,[93] silicon,[94] Cn−In−S,[95] ZnSe,[96] and colloidal graphene QDs.[97,98] The lattice mismatch in QDs mentioned above usually leads to plenty of surface trap states and low EQEs. However, Cd-free cg-QDs with nearly free lattice mismatch promise to have superior performance. Kim et al. fabricated efficient and stable blue QLEDs by designing and utilizing continuously graded ZnTeSe/ZnSe/ZnS QDs (top panel in Figure 8d).[99] In addition, after a two-step ligand exchange process to passivate the trapping sites and stacking faults in QDs, the EQE of the blue LEDs could reach as high as 20.2% with good operational stabilities (T_{50} = 442 h at 650 cd m^{-2}) (bottom panel in Figure 8d).

Despite the achievements discussed above, the synthesis of Cd-free QDs is still immature; therefore, their performance is barely satisfactory in comparison to that of Cd-QDs. With the numerous explorations and progress in chemical synthesis of Cd-free cg-QDs, it will promise to promote the further development of Cd-free QDs in LED applications.

The emergence of cg-QDs combined with device-architecture engineering is expected to remedy the remaining defects in QLEDs, such as the efficiency roll-off behavior, short device lifetimes under high brightness, and low brightness at around the bandgap. Together with other figures of merit, including high efficiency, high brightness, and pure color, the well-designed high-quality cg-QDs will motivate novel applications of QLEDs toward cost-effective, environmentally-friendly, energy-saving, and white-color-gamut displays. We expect the road toward the optimized synthesis of large-size and defect-free cg-QDs will further promote the development of next-generation display technologies.

AUTHOR INFORMATION

Corresponding Authors

Hao Hong − *State Key Laboratory for Mesoscopic Physics, Frontiers Science Center for Nano-optoelectronics, School of Physics, Peking University, Beijing 100871, China*; Email: haohong@pku.edu.cn

Kaihui Liu − *State Key Laboratory for Mesoscopic Physics, Frontiers Science Center for Nano-optoelectronics, School of Physics and International Center for Quantum Materials, Collaborative Innovation Center of Quantum Matter, Peking University, Beijing 100871, China*; orcid.org/0000-0002-8781-2495; Email: khliu@pku.edu.cn

Huaibin Shen − *Key Laboratory for Special Functional Materials, Ministry of Education, School of Materials Science and Engineering, Henan University, Kaifeng 475004, China*; orcid.org/0000-0002-6425-0514; Email: shenhuaibin@henu.edu.cn

https://doi.org/10.1021/acs.jpclett.1c01554
J. Phys. Chem. Lett. 2021, 12, 5967−5978

Authors

Yang Cheng − *State Key Laboratory for Mesoscopic Physics, Frontiers Science Center for Nano-optoelectronics, School of Physics, Peking University, Beijing 100871, China; Key Laboratory for Special Functional Materials, Ministry of Education, School of Materials Science and Engineering, Henan University, Kaifeng 475004, China;* orcid.org/0000-0003-2925-8606

Haoyue Wan − *State Key Laboratory for Mesoscopic Physics, Frontiers Science Center for Nano-optoelectronics, School of Physics, Peking University, Beijing 100871, China*

Tianyu Liang − *State Key Laboratory for Mesoscopic Physics, Frontiers Science Center for Nano-optoelectronics, School of Physics, Peking University, Beijing 100871, China*

Can Liu − *State Key Laboratory for Mesoscopic Physics, Frontiers Science Center for Nano-optoelectronics, School of Physics, Peking University, Beijing 100871, China;* orcid.org/0000-0001-5451-4144

Muhong Wu − *International Center for Quantum Materials, Collaborative Innovation Center of Quantum Matter and Interdisciplinary Institute of Light-Element Quantum Materials and Research Center for Light-Element Advanced Materials, Peking University, Beijing 100871, China; Songshan Lake Laboratory for Materials Science, Dongguan 523808, China*

Complete contact information is available at: https://pubs.acs.org/10.1021/acs.jpclett.1c01554

Notes

The authors declare no competing financial interest.

■ ACKNOWLEDGMENTS

This work was supported by the Key R&D Program of Guangdong Province (2020B010189001, 2019B010931001, and 2018B030327001), the National Natural Science Foundation of China (52025023, 51991342, 52021006, 11888101, 61874039, and 61922028), the Strategic Priority Research Program of Chinese Academy of Sciences (XDB33000000), Beijing Natural Science Foundation (JQ19004), Beijing Excellent Talents Training Support (2017000026833ZK11), the Pearl River Talent Recruitment Program of Guangdong Province (2019ZT08C321), and the China Postdoctoral Science Foundation (2020M680177).

■ REFERENCES

(1) Brus, L. E. Electron-electron and electron-hole interactions in small semiconductor crystallites: the size dependence of the lowest excited electronic state. *J. Chem. Phys.* **1984**, *80*, 4403−4409.

(2) Murray, C.; Norris, D. J.; Bawendi, M. G. Synthesis and characterization of nearly monodisperse CdE (E= sulfur, selenium, tellurium) semiconductor nanocrystallites. *J. Am. Chem. Soc.* **1993**, *115*, 8706−8715.

(3) Alivisatos, A. P. Semiconductor clusters, nanocrystals, and quantum dots. *Science* **1996**, *271*, 933−937.

(4) Pu, C.; Qin, H.; Gao, Y.; Zhou, J.; Wang, P.; Peng, X. Synthetic control of exciton behavior in colloidal quantum dots. *J. Am. Chem. Soc.* **2017**, *139*, 3302−3311.

(5) Liu, A.; Almeida, D. B.; Bae, W.-K.; Padilha, L. A.; Cundiff, S. T. Simultaneous existence of confined and delocalized vibrational modes in colloidal quantum dots. *J. Phys. Chem. Lett.* **2019**, *10*, 6144−6150.

(6) Kim, J. Y.; Voznyy, O.; Zhitomirsky, D.; Sargent, E. H. 25th anniversary article: colloidal quantum dot materials and devices: a quarter-century of advances. *Adv. Mater.* **2013**, *25*, 4986−5010.

(7) Kagan, C. R.; Lifshitz, E.; Sargent, E. H.; Talapin, D. V. Building devices from colloidal quantum dots. *Science* **2016**, *353*, aac5523.

(8) Colvin, V. L.; Schlamp, M. C.; Alivisatos, A. P. Light-emitting diodes made from cadmium selenide nanocrystals and a semiconducting polymer. *Nature* **1994**, *370*, 354−357.

(9) Coe, S.; Woo, W.-K.; Bawendi, M.; Bulović, V. Electroluminescence from single monolayers of nanocrystals in molecular organic devices. *Nature* **2002**, *420*, 800−803.

(10) Sun, Q.; Wang, Y. A.; Li, L. S.; Wang, D.; Zhu, T.; Xu, J.; Yang, C.; Li, Y. Bright, multicoloured light-emitting diodes based on quantum dots. *Nat. Photonics* **2007**, *1*, 717−722.

(11) Cho, K.-S.; Lee, E. K.; Joo, W.-J.; Jang, E.; Kim, T.-H.; Lee, S. J.; Kwon, S.-J.; Han, J. Y.; Kim, B.-K.; Choi, B. L.; et al. High-performance crosslinked colloidal quantum-dot light-emitting diodes. *Nat. Photonics* **2009**, *3*, 341−345.

(12) Jang, E.; Jun, S.; Jang, H.; Lim, J.; Kim, B.; Kim, Y. White-light-emitting diodes with quantum dot color converters for display backlights. *Adv. Mater.* **2010**, *22*, 3076−3080.

(13) Qian, L.; Zheng, Y.; Xue, J.; Holloway, P. H. Stable and efficient quantum-dot light-emitting diodes based on solution-processed multilayer structures. *Nat. Photonics* **2011**, *5*, 543−548.

(14) Dai, X.; Zhang, Z.; Jin, Y.; Niu, Y.; Cao, H.; Liang, X.; Chen, L.; Wang, J.; Peng, X. Solution-processed, high-performance light-emitting diodes based on quantum dots. *Nature* **2014**, *515*, 96−99.

(15) Shen, H.; Gao, Q.; Zhang, Y.; Lin, Y.; Lin, Q.; Li, Z.; Chen, L.; Zeng, Z.; Li, X.; Jia, Y.; et al. Visible quantum dot light-emitting diodes with simultaneous high brightness and efficiency. *Nat. Photonics* **2019**, *13*, 192−197.

(16) Shmshad, A.; Tang, J.; Muhammad, I.; Han, D.; Zhang, X.; Chang, S.; Shi, Q.; Zhong, H. Illustrating the shell thickness dependence in alloyed core/shell quantum-dot-based light-emitting diodes by impedance spectroscopy. *J. Phys. Chem. C* **2019**, *123*, 26011−26017.

(17) Li, B.; Lu, M.; Feng, J.; Zhang, J.; Smowton, P. M.; Sohn, J. I.; Park, I.-K.; Zhong, H.; Hou, B. Colloidal quantum dot hybrids: an emerging class of materials for ambient lighting. *J. Mater. Chem. C* **2020**, *8*, 10676−10695.

(18) Shirasaki, Y.; Supran, G. J.; Tisdale, W. A.; Bulović, V. Origin of efficiency roll-off in colloidal quantum-dot light-emitting diodes. *Phys. Rev. Lett.* **2013**, *110*, 217403.

(19) Bozyigit, D.; Yarema, O.; Wood, V. Origins of low quantum efficiencies in quantum dot LEDs. *Adv. Funct. Mater.* **2013**, *23*, 3024−3029.

(20) Klimov, V. I. Multicarrier interactions in semiconductor nanocrystals in relation to the phenomena of Auger recombination and carrier multiplication. *Annu. Rev. Condens. Matter Phys.* **2014**, *5*, 285−316.

(21) Kwak, J.; Bae, W. K.; Lee, D.; Park, I.; Lim, J.; Park, M.; Cho, H.; Woo, H.; Yoon, D. Y.; Char, K.; et al. Bright and efficient full-color colloidal quantum dot light-emitting diodes using an inverted device structure. *Nano Lett.* **2012**, *12*, 2362−2366.

(22) Cho, J.; Schubert, E. F.; Kim, J. K. Efficiency droop in light-emitting diodes: Challenges and countermeasures. *Laser Photonics Rev.* **2013**, *7*, 408−421.

(23) Mashford, B. S.; Stevenson, M.; Popovic, Z.; Hamilton, C.; Zhou, Z.; Breen, C.; Steckel, J.; Bulovic, V.; Bawendi, M.; Coe-Sullivan, S.; et al. High-efficiency quantum-dot light-emitting devices with enhanced charge injection. *Nat. Photonics* **2013**, *7*, 407−412.

(24) Supran, G. J.; Shirasaki, Y.; Song, K. W.; Caruge, J.-M.; Kazlas, P. T.; Coe-Sullivan, S.; Andrew, T. L.; Bawendi, M. G.; Bulović, V. QLEDs for displays and solid-state lighting. *MRS Bull.* **2013**, *38*, 703−711.

(25) Bae, W. K.; Park, Y.-S.; Lim, J.; Lee, D.; Padilha, L. A.; McDaniel, H.; Robel, I.; Lee, C.; Pietryga, J. M.; Klimov, V. I. Controlling the influence of Auger recombination on the performance of quantum-dot light-emitting diodes. *Nat. Commun.* **2013**, *4*, 2661.

(26) Park, Y.-S.; Bae, W. K.; Baker, T.; Lim, J.; Klimov, V. I. Effect of Auger recombination on lasing in heterostructured quantum dots with engineered core/shell interfaces. *Nano Lett.* **2015**, *15*, 7319−7328.

(27) Fan, F.; Voznyy, O.; Sabatini, R. P.; Bicanic, K. T.; Adachi, M. M.; McBride, J. R.; Reid, K. R.; Park, Y.-S.; Li, X.; Jain, A.; et al. Continuous-wave lasing in colloidal quantum dot solids enabled by facet-selective epitaxy. *Nature* **2017**, *544*, 75−79.
(28) Mahler, B.; Spinicelli, P.; Buil, S.; Quelin, X.; Hermier, J.-P.; Dubertret, B. Towards non-blinking colloidal quantum dots. *Nat. Mater.* **2008**, *7*, 659−664.
(29) Chen, Y.; Vela, J.; Htoon, H.; Casson, J. L.; Werder, D. J.; Bussian, D. A.; Klimov, V. I.; Hollingsworth, J. A. Giant" multishell CdSe nanocrystal quantum dots with suppressed blinking. *J. Am. Chem. Soc.* **2008**, *130*, 5026−5027.
(30) Norris, D. J.; Efros, A. L.; Erwin, S. C. Doped nanocrystals. *Science* **2008**, *319*, 1776−1779.
(31) Htoon, H.; Malko, A. V.; Bussian, D.; Vela, J.; Chen, Y.; Hollingsworth, J. A.; Klimov, V. I. Highly emissive multiexcitons in steady-state photoluminescence of individual "giant" CdSe/CdS core/shell nanocrystals. *Nano Lett.* **2010**, *10*, 2401−2407.
(32) Yang, Y.; Zheng, Y.; Cao, W.; Titov, A.; Hyvonen, J.; Manders, J. R.; Xue, J.; Holloway, P. H.; Qian, L. High-efficiency light-emitting devices based on quantum dots with tailored nanostructures. *Nat. Photonics* **2015**, *9*, 259−266.
(33) Li, Z.; Hu, Y.; Shen, H.; Lin, Q.; Wang, L.; Wang, H.; Zhao, W.; Li, L. S. Efficient and long-life green light-emitting diodes comprising tridentate thiol capped quantum dots. *Laser Photonics Rev.* **2017**, *11*, 1600227.
(34) Rhee, S.; Chang, J. H.; Hahm, D.; Jeong, B. G.; Kim, J.; Lee, H.; Lim, J.; Hwang, E.; Kwak, J.; Bae, W. K. Tailoring the electronic landscape of quantum dot light-emitting diodes for high brightness and stable operation. *ACS Nano* **2020**, *14*, 17496−17504.
(35) Philbin, J. P.; Rabani, E. Auger recombination lifetime scaling for type I and quasi-type II core/shell quantum dots. *J. Phys. Chem. Lett.* **2020**, *11*, 5132−5138.
(36) Cragg, G. E.; Efros, A. L. Suppression of Auger processes in confined structures. *Nano Lett.* **2010**, *10*, 313−317.
(37) Efros, A. L.; Nesbitt, D. J. Origin and control of blinking in quantum dots. *Nat. Nanotechnol.* **2016**, *11*, 661−671.
(38) Wu, K.; Park, Y.-S.; Lim, J.; Klimov, V. I. Towards zero-threshold optical gain using charged semiconductor quantum dots. *Nat. Nanotechnol.* **2017**, *12*, 1140−1147.
(39) Shen, H.; Bai, X.; Wang, A.; Wang, H.; Qian, L.; Yang, Y.; Titov, A.; Hyvonen, J.; Zheng, Y.; Li, L. S. High-efficient deep-blue light-emitting diodes by using high quality $Zn_xCd_{1-x}S$/ZnS core/shell quantum dots. *Adv. Funct. Mater.* **2014**, *24*, 2367−2373.
(40) Shen, H.; Cao, W.; Shewmon, N. T.; Yang, C.; Li, L. S.; Xue, J. High-efficiency, low turn-on voltage blue-violet quantum-dot-based light-emitting diodes. *Nano Lett.* **2015**, *15*, 1211−1216.
(41) Song, J.; Wang, O.; Shen, H.; Lin, Q.; Li, Z.; Wang, L.; Zhang, X.; Li, L. S. Over 30% external quantum efficiency light-emitting diodes by engineering quantum dot-assisted energy level match for hole transport layer. *Adv. Funct. Mater.* **2019**, *29*, 1808377.
(42) Bae, W. K.; Char, K.; Hur, H.; Lee, S. Single-step synthesis of quantum dots with chemical composition gradients. *Chem. Mater.* **2008**, *20*, 531−539.
(43) Bae, W. K.; Kwak, J.; Park, J. W.; Char, K.; Lee, C.; Lee, S. Highly efficient green-light-emitting diodes based on CdSe@ ZnS quantum dots with a chemical-composition gradient. *Adv. Mater.* **2009**, *21*, 1690−1694.
(44) Shen, H.; Zhou, C.; Xu, S.; Yu, C.; Wang, H.; Chen, X.; Li, L. S. Phosphine-free synthesis of $Zn_{1-x}Cd_xSe$/ZnSe/$ZnSe_xS_{1-x}$/ZnS core/multishell structures with bright and stable blue-green photoluminescence. *J. Mater. Chem.* **2011**, *21*, 6046−6053.
(45) Shen, H.; Wang, H.; Zhou, C.; Niu, J. Z.; Yuan, H.; Ma, L.; Li, L. S. Large scale synthesis of stable tricolor $Zn_{1-x}Cd_xSe$ core/multishell nanocrystals via a facile phosphine-free colloidal method. *Dalton Trans.* **2011**, *40*, 9180−9188.
(46) Lim, J.; Jeong, B. G.; Park, M.; Kim, J. K.; Pietryga, J. M.; Park, Y. S.; Klimov, V. I.; Lee, C.; Lee, D. C.; Bae, W. K. Influence of shell thickness on the performance of light-emitting devices based on $CdSe/Zn_{1-X}Cd_XS$ core/shell heterostructured quantum dots. *Adv. Mater.* **2014**, *26*, 8034−8040.
(47) Bae, W. K.; Nam, M. K.; Char, K.; Lee, S. Gram-scale one-pot synthesis of highly luminescent blue emitting $Cd_{1-x}Zn_xS$/ZnS nanocrystals. *Chem. Mater.* **2008**, *20*, 5307−5313.
(48) Lim, J.; Park, Y.-S.; Klimov, V. I. Optical gain in colloidal quantum dots achieved with direct-current electrical pumping. *Nat. Mater.* **2018**, *17*, 42−49.
(49) Lim, J.; Park, Y.-S.; Wu, K.; Yun, H. J.; Klimov, V. I. Droop-free colloidal quantum dot light emitting diodes. *Nano Lett.* **2018**, *18*, 6645−6653.
(50) Bae, W. K.; Padilha, L. A.; Park, Y.-S.; McDaniel, H.; Robel, I.; Pietryga, J. M.; Klimov, V. I. Controlled alloying of the core−shell interface in CdSe/CdS quantum dots for suppression of Auger recombination. *ACS Nano* **2013**, *7*, 3411−3419.
(51) Park, Y.-S.; Bae, W. K.; Padilha, L. A.; Pietryga, J. M.; Klimov, V. I. Effect of the core/shell interface on Auger recombination evaluated by single-quantum-dot spectroscopy. *Nano Lett.* **2014**, *14*, 396−402.
(52) Park, Y.-S.; Bae, W. K.; Pietryga, J. M.; Klimov, V. I. Auger recombination of biexcitons and negative and positive trions in individual quantum dots. *ACS Nano* **2014**, *8*, 7288−7296.
(53) Park, Y.-S.; Lim, J.; Makarov, N. S.; Klimov, V. I. Effect of interfacial alloying versus "volume scaling" on Auger recombination in compositionally graded semiconductor quantum dots. *Nano Lett.* **2017**, *17*, 5607−5613.
(54) García-Santamaría, F.; Chen, Y.; Vela, J.; Schaller, R. D.; Hollingsworth, J. A.; Klimov, V. I. Suppressed auger recombination in "giant" nanocrystals boosts optical gain performance. *Nano Lett.* **2009**, *9*, 3482−3488.
(55) Tang, J.; Huang, S.; Li, Z.; Shen, H.; Lv, Z.; Zhong, H. Morphology evolution of gradient-alloyed $Cd_xZn_{1-x}Se_yS_{1-y}$@ ZnS core-shell quantum dots during transmission electron microscopy determination: a route to illustrate strain effects. *J. Phys. Chem. C* **2018**, *122*, 4583−4588.
(56) Efros, A. L. Almost always bright. *Nat. Mater.* **2008**, *7*, 612−613.
(57) Nirmal, M.; Dabbousi, B. O.; Bawendi, M. G.; Macklin, J. J.; Trautman, J. K.; Harris, T. D.; Brus, L. E. Fluorescence intermittency in single cadmium selenide nanocrystals. *Nature* **1996**, *383*, 802−804.
(58) Chen, O.; Zhao, J.; Chauhan, V. P.; Cui, J.; Wong, C.; Harris, D. K.; Wei, H.; Han, H.-S.; Fukumura, D.; Jain, R. K.; et al. Compact high-quality CdSe-CdS core-shell nanocrystals with narrow emission linewidths and suppressed blinking. *Nat. Mater.* **2013**, *12*, 445−451.
(59) Peng, X.; Schlamp, M. C.; Kadavanich, A. V.; Alivisatos, A. P. Epitaxial growth of highly luminescent CdSe/CdS core/shell nanocrystals with photostability and electronic accessibility. *J. Am. Chem. Soc.* **1997**, *119*, 7019−7029.
(60) Kim, S.; Fisher, B.; Eisler, H.-J.; Bawendi, M. Type-II quantum dots: CdTe/CdSe (core/shell) and CdSe/ZnTe (core/shell) heterostructures. *J. Am. Chem. Soc.* **2003**, *125*, 11466−11467.
(61) Beane, G. A.; Gong, K.; Kelley, D. F. Auger and carrier trapping dynamics in core/shell quantum dots having sharp and alloyed interfaces. *ACS Nano* **2016**, *10*, 3755−3765.
(62) Wang, X.; Ren, X.; Kahen, K.; Hahn, M. A.; Rajeswaran, M.; Maccagnano-Zacher, S.; Silcox, J.; Cragg, G. E.; Efros, A. L.; Krauss, T. D. Non-blinking semiconductor nanocrystals. *Nature* **2009**, *459*, 686−689.
(63) Qin, W.; Shah, R. A.; Guyot-Sionnest, P. CdSeS/ZnS alloyed nanocrystal lifetime and blinking studies under electrochemical control. *ACS Nano* **2012**, *6*, 912−918.
(64) Nasilowski, M.; Spinicelli, P.; Patriarche, G.; Dubertret, B. Gradient CdSe/CdS quantum dots with room temperature biexciton unity quantum yield. *Nano Lett.* **2015**, *15*, 3953−3958.
(65) Guo, W.; Tang, J.; Zhang, G.; Li, B.; Yang, C.; Chen, R.; Qin, C.; Hu, J.; Zhong, H.; Xiao, L.; et al. Photoluminescence blinking and biexciton Auger recombination in single colloidal quantum dots with sharp and smooth core/shell interfaces. *J. Phys. Chem. Lett.* **2021**, *12*, 405−412.

https://doi.org/10.1021/acs.jpclett.1c01554
J. Phys. Chem. Lett. 2021, 12, 5967−5978

(66) Bae, W. K.; Brovelli, S.; Klimov, V. I. Spectroscopic insights into the performance of quantum dot light-emitting diodes. *MRS Bull.* **2013**, *38*, 721−730.
(67) Pietryga, J. M.; Park, Y.-S.; Lim, J.; Fidler, A. F.; Bae, W. K.; Brovelli, S.; Klimov, V. I. Spectroscopic and device aspects of nanocrystal quantum dots. *Chem. Rev.* **2016**, *116*, 10513−10622.
(68) Li, Y.; Rizzo, A.; Cingolani, R.; Gigli, G. Bright white-light-emitting device from ternary nanocrystal composites. *Adv. Mater.* **2006**, *18*, 2545−2548.
(69) Anikeeva, P. O.; Halpert, J. E.; Bawendi, M. G.; Bulović, V. Electroluminescence from a mixed red-green-blue colloidal quantum dot monolayer. *Nano Lett.* **2007**, *7*, 2196−2200.
(70) Lee, K.-H.; Han, C.-Y.; Kang, H.-D.; Ko, H.; Lee, C.; Lee, J.; Myoung, N.; Yim, S.-Y.; Yang, H. Highly efficient, color-reproducible full-color electroluminescent devices based on red/green/blue quantum dot-mixed multilayer. *ACS Nano* **2015**, *9*, 10941−10949.
(71) Achermann, M.; Bartko, A. P.; Hollingsworth, J. A.; Klimov, V. I. The effect of Auger heating on intraband carrier relaxation in semiconductor quantum rods. *Nat. Phys.* **2006**, *2*, 557−561.
(72) Scholz, S.; Kondakov, D.; Lussem, B.; Leo, K. Degradation mechanisms and reactions in organic light-emitting devices. *Chem. Rev.* **2015**, *115*, 8449−8503.
(73) Deng, Y.; Lin, X.; Fang, W.; Di, D.; Wang, L.; Friend, R. H.; Peng, X.; Jin, Y. Deciphering exciton-generation processes in quantum-dot electroluminescence. *Nat. Commun.* **2020**, *11*, 2309.
(74) Zhang, W.; Chen, X.; Ma, Y.; Xu, Z.; Wu, L.; Yang, Y.; Tsang, S.-W.; Chen, S. Positive aging effect of ZnO nanoparticles induced by surface stabilization. *J. Phys. Chem. Lett.* **2020**, *11*, 5863−5870.
(75) Klimov, V.; Mikhailovsky, A.; Xu, S.; Malko, A.; Hollingsworth, J.; Leatherdale, a. C.; Eisler, H.-J.; Bawendi, M. Optical gain and stimulated emission in nanocrystal quantum dots. *Science* **2000**, *290*, 314−317.
(76) Dang, C.; Lee, J.; Breen, C.; Steckel, J. S.; Coe-Sullivan, S.; Nurmikko, A. Red, green and blue lasing enabled by single-exciton gain in colloidal quantum dot films. *Nat. Nanotechnol.* **2012**, *7*, 335−339.
(77) Vandyshev, Y. V.; Dneprovskii, V.; Klimov, V.; Okorokov, D. Lasing on a transition between quantum-well levels in a quantum dot. *JETP Lett.* **1991**, *54*, 442.
(78) Park, Y.-S.; Roh, J.; Diroll, B. T.; Schaller, R. D.; Klimov, V. I. Colloidal quantum dot lasers. *Nat. Rev. Mater.* **2021**, *6*, 382−401.
(79) Kozlov, O. V.; Park, Y.-S.; Roh, J.; Fedin, I.; Nakotte, T.; Klimov, V. I. Sub-single-exciton lasing using charged quantum dots coupled to a distributed feedback cavity. *Science* **2019**, *365*, 672−675.
(80) Klimov, V. I.; Mikhailovsky, A. A.; McBranch, D.; Leatherdale, C. A.; Bawendi, M. G. Quantization of multiparticle Auger rates in semiconductor quantum dots. *Science* **2000**, *287*, 1011−1013.
(81) Roh, J.; Park, Y.-S.; Lim, J.; Klimov, V. I. Optically pumped colloidal-quantum-dot lasing in LED-like devices with an integrated optical cavity. *Nat. Commun.* **2020**, *11*, 271.
(82) Cordero, S.; Carson, P.; Estabrook, R.; Strouse, G.; Buratto, S. Photo-activated luminescence of CdSe quantum dot monolayers. *J. Phys. Chem. B* **2000**, *104*, 12137−12142.
(83) Jones, M.; Nedeljkovic, J.; Ellingson, R. J.; Nozik, A. J.; Rumbles, G. Photoenhancement of luminescence in colloidal CdSe quantum dot solutions. *J. Phys. Chem. B* **2003**, *107*, 11346−11352.
(84) Dembski, S.; Graf, C.; Krüger, T.; Gbureck, U.; Ewald, A.; Bock, A.; Rühl, E. Photoactivation of CdSe/ZnS quantum dots embedded in silica colloids. *Small* **2008**, *4*, 1516−1526.
(85) Jain, A.; Voznyy, O.; Korkusinski, M.; Hawrylak, P.; Sargent, E. H. Ultrafast carrier trapping in thick-shell colloidal quantum dots. *J. Phys. Chem. Lett.* **2017**, *8*, 3179−3184.
(86) Grenland, J. J.; Maddux, C. J.; Kelley, D. F.; Kelley, A. M. Charge trapping versus exciton delocalization in CdSe quantum dots. *J. Phys. Chem. Lett.* **2017**, *8*, 5113−5118.
(87) Chang, J. H.; Park, P.; Jung, H.; Jeong, B. G.; Hahm, D.; Nagamine, G.; Ko, J.; Cho, J.; Padilha, L. A.; Lee, D. C.; et al. Unraveling the origin of operational instability of quantum dot based light-emitting diodes. *ACS Nano* **2018**, *12*, 10231−10239.
(88) Rhee, S.; Chang, J. H.; Hahm, D.; Kim, K.; Jeong, B. G.; Lee, H. J.; Lim, J.; Char, K.; Lee, C.; Bae, W. K. Positive incentive" approach to enhance the operational stability of quantum dot-based light-emitting diodes. *ACS Appl. Mater. Interfaces* **2019**, *11*, 40252−40259.
(89) Chen, J.; Wang, J.; Xu, X.; Li, J.; Song, J.; Lan, S.; Liu, S.; Cai, B.; Han, B.; Precht, J. T.; et al. Efficient and bright white light-emitting diodes based on single-layer heterophase halide perovskites. *Nat. Photonics* **2021**, *15*, 238−244.
(90) Jiang, C.; Zou, J.; Liu, Y.; Song, C.; He, Z.; Zhong, Z.; Wang, J.; Yip, H.-L.; Peng, J.; Cao, Y. Fully solution-processed tandem white quantum-dot light-emitting diode with an external quantum efficiency exceeding 25%. *ACS Nano* **2018**, *12*, 6040−6049.
(91) Zhang, H.; Su, Q.; Sun, Y.; Chen, S. Efficient and color stable white quantum-dot light-emitting diodes with external quantum efficiency over 23%. *Adv. Opt. Mater.* **2018**, *6*, 1800354.
(92) Derfus, A. M.; Chan, W. C.; Bhatia, S. N. Probing the cytotoxicity of semiconductor quantum dots. *Nano Lett.* **2004**, *4*, 11−18.
(93) Lim, J.; Park, M.; Bae, W. K.; Lee, D.; Lee, S.; Lee, C.; Char, K. Highly efficient cadmium-free quantum dot light-emitting diodes enabled by the direct formation of excitons within InP@ ZnSeS quantum dots. *ACS Nano* **2013**, *7*, 9019−9026.
(94) Maier-Flaig, F.; Rinck, J.; Stephan, M.; Bocksrocker, T.; Bruns, M.; Kübel, C.; Powell, A. K.; Ozin, G. A.; Lemmer, U. Multicolor silicon light-emitting diodes (SiLEDs). *Nano Lett.* **2013**, *13*, 475−480.
(95) Kim, J.-H.; Yang, H. High-efficiency Cu-In-S quantum-dot-light-emitting device exceeding 7%. *Chem. Mater.* **2016**, *28*, 6329−6335.
(96) Ji, W.; Jing, P.; Xu, W.; Yuan, X.; Wang, Y.; Zhao, J.; Jen, A. K.-Y. High color purity ZnSe/ZnS core/shell quantum dot based blue light emitting diodes with an inverted device structure. *Appl. Phys. Lett.* **2013**, *103*, 053106.
(97) Li, L.-s.; Yan, X. Colloidal graphene quantum dots. *J. Phys. Chem. Lett.* **2010**, *1*, 2572−2576.
(98) Ghosh, S.; Oleksiievets, N.; Enderlein, J. r.; Chizhik, A. I. Emission states variation of single graphene quantum dots. *J. Phys. Chem. Lett.* **2020**, *11*, 7356−7362.
(99) Kim, T.; Kim, K.-H.; Kim, S.; Choi, S.-M.; Jang, H.; Seo, H.-K.; Lee, H.; Chung, D.-Y.; Jang, E. Efficient and stable blue quantum dot light-emitting diode. *Nature* **2020**, *586*, 385−389.

https://doi.org/10.1021/acs.jpclett.1c01554
J. Phys. Chem. Lett. 2021, 12, 5967−5978